

Density-functional study of Mn monosilicide on the Si(111) surface: Film formation versus island nucleation

Mahbube Hortamani,¹ Peter Kratzer,^{1,2} and Matthias Scheffler¹

¹*Fritz-Haber-Institut der Max-Planck-Gesellschaft, Faradayweg 4-6, D-14195 Berlin, Germany*

²*Fachbereich Physik, Universität Duisburg-Essen, Lotharstrasse 1, D-47048 Duisburg, Germany*

(Received 10 July 2007; revised manuscript received 29 October 2007; published 26 December 2007)

The stability of thin films and of small crystallites of Mn monosilicide (MnSi) on the Si(111) surface is investigated by density-functional theory calculations. Extending previous studies of MnSi/Si(001), our calculations indicate that MnSi films on Si(111) have similar electronic and magnetic properties, i.e., large magnetic moments at the Mn atoms near the surfaces and interfaces and a high degree of spin polarization at the Fermi level. Hence, such MnSi films could be interesting as a spintronics material compatible with silicon. Moreover, from our calculated total energies we conclude that the Si(111) substrate should be more suitable to grow MnSi layers than the Si(001) substrate. This result is obtained by analyzing the conditions for the formation of three-dimensional (3D) MnSi islands, either in the *B20* crystal structure or as pseudomorphic islands in the *B2* structure: On Si(001), 3D islands, even if they are just a few lattice constants wide, are found to be already more stable than a homogeneous MnSi film. A bipyramidal “iceberg” island consisting of MnSi in the *B20* structure on the Si(001) substrate is found to be most stable among the structures investigated. For MnSi on Si(111), however, our calculations show that the nucleus for forming a 3D island is larger. Therefore, Mn deposition initially leads to the formation of flat 2D islands. On Si(111), the lowest-energy structure for such islands is found to be similar to the *B20* structure of bulk MnSi, whereas on Si(001) this structure is incompatible with the substrate lattice. Our results are in agreement with the experimental observations, formation of an almost closed film with $(\sqrt{3} \times \sqrt{3})$ structure on Si(111), and 3D island formation on Si(001).

DOI: [10.1103/PhysRevB.76.235426](https://doi.org/10.1103/PhysRevB.76.235426)

PACS number(s): 68.43.Bc, 68.55.Ac, 75.70.-i

I. INTRODUCTION

The injection of a spin-polarized electric current from a ferromagnet into a semiconductor is one of the key challenges in present-day spintronics research. Some progress towards this goal has been made by growing epitaxial films of Fe or Fe₃Si on GaAs and InAs substrates.¹⁻⁴ However, on the most common semiconductor substrate silicon, growth of magnetic films of Fe or Co with the quality required for efficient spin injectors has not been achieved up to now. In most cases, a transition metal silicide is formed instead of the desired metal film. This is in contrast to Fe on GaAs, where metallic Fe films were obtained. The silicides formed on Si, e.g., bulk FeSi and CoSi₂, are nonmagnetic and thus useless for building spintronics devices. Interestingly, some monosilicides, such as CoSi and MnSi, are ferromagnetic as thin films in the pseudomorphic *B2* (cesium-chloride) crystal structure, as we showed recently by density-functional calculations.^{5,6} Moreover, MnSi in the hypothetical zincblende structure is predicted to be ferromagnetic by DFT calculations.⁷ While calculations for MnSi films on Si(001) have been presented recently,^{5,8} the present paper deals with thin films and islands of MnSi on Si(111). Our present calculations suggest that the Si(111) substrate is more suitable than Si(001) for growing MnSi overlayers. Results for thin layers with either the ground-state crystal structure of MnSi (the so-called *B20* structure), or the *B2* structure are compared. Moreover, special attention is given to the possibility of three-dimensional island formation. While we find the tendency to island formation to be very strong for MnSi/Si(001), the three-dimensional islands on Si(111) only become stable above a certain size, according to our calcu-

lations. Thus, the preferred substrate for growing layers of MnSi should be Si(111). The previously studied system MnSi/Si(001) could be an interesting system for preparing and studying ferromagnetic or superparamagnetic MnSi nanostructures.

By depositing Mn either on Si(111) or Si(001), silicides with varying stoichiometry have been obtained experimentally, such as MnSi_{1.7},⁹ MnSi,¹⁰ or Mn₅Si₃,¹¹ depending on the growth conditions. In this study, we restrict ourselves to the epitaxial growth of Mn monosilicide (MnSi), and investigate which substrate orientation of silicon is promising to grow thin films of MnSi. Experimentally, MnSi films on Si(111) have been grown both with and without Bi as a surfactant.¹¹⁻¹⁷ Surface structural phase transitions,¹⁸ as well as a nonmetal-to-metal phase transition in 5–10 monolayers (ML) thick films¹⁹ have been reported. Evans, Glueckstein, and Nogami observed by low-energy electron diffraction (LEED) and by scanning-tunneling microscopy (STM) that deposition of Mn on Si(111) first leads to formation of large, flat islands (diameter several tens of nanometer) displaying a $(\sqrt{3} \times \sqrt{3})$ reconstruction.¹² Above about four monolayers of Mn, these islands almost completely cover the surface. These findings were confirmed by Kumar *et al.*²⁰ using similar techniques. Likewise, flat-top islands with $(\sqrt{3} \times \sqrt{3})$ structure were observed by Azatyan, Iwami, and Lifshits after depositing submonolayers of Mn on Si(111)(7×7) and annealing to 450 °C.²¹ Moreover, this characteristic $(\sqrt{3} \times \sqrt{3})$ pattern has been used to identify side facets of MnSi islands on Si(001) as MnSi(111) facets.²² So far, no atomistic model of the $(\sqrt{3} \times \sqrt{3})$ reconstruction has been presented in the literature, and even its relation to the bulk crystal structure of MnSi has remained unclear. In this paper, we suggest an

atomistic model for the $(\sqrt{3} \times \sqrt{3})$ structure for thin MnSi films derived from the $B20$ structure of bulk MnSi. The magnetic properties are studied both for these $B20$ -like films and for films with a simpler, $B2$ -like structure on Si(111) in order to make contact to the previously studied $B2$ -like films on Si(001).

This paper is arranged as follows. Section II provides the technical details of the method used, mainly intended for those who want to reproduce the calculations. In Sec. III, we discuss the structure, the thermodynamic stability and the magnetic properties of MnSi films on Si(111). Formation of crystallites with certain shapes (pyramid or bipyramid) and sizes is considered in Sec. IV. A summary and conclusions follow in Sec. V.

II. CALCULATIONS

In this work, we calculate the atomic structure, the stability, and the electronic and magnetic properties of thin manganese silicide films using density-functional theory (DFT). The electronic exchange and correlation is treated within the generalized gradient approximation (GGA-PBE).²³ We perform all-electron calculations using the full-potential augmented plane wave plus local orbital (FP-APW+LO) method implemented in the WIEN2K code.²⁴ In all calculations, the muffin-tin sphere radius is chosen to be 1.11 Å for both Mn and Si. Inside the muffin-tin spheres, wave functions, electron density and potential are expanded in spherical harmonics up to angular momentum quantum numbers $l_{\max}^{\text{WF}} = 12$ and $l_{\max}^{\text{pot}} = 6$, respectively. In the interstitial region a plane-wave expansion with a cutoff energy of $E_{\text{cut}}^{\text{WF}} = 13.8$ Ry is used. Repeated slab geometries are used to describe the surfaces and interfaces in this study. The lateral dimensions of the unit cell are determined by the bulk lattice constant of silicon, calculated to be 5.47 Å within the GGA-PBE functional. For Si(111) (1×1), the Brillouin zone sampling is done by a set of 12 k points in the irreducible part of the Brillouin zone, derived from a $9 \times 9 \times 1$ k -point mesh. For the larger Si(111) $(\sqrt{3} \times \sqrt{3})$ unit cell, a coarser k -point mesh of $6 \times 6 \times 1$ k points is used. For calculations for Si(001) surfaces and thin films, the quality of Brillouin sampling corresponds to $8 \times 8 \times 1$ k points in the Brillouin zone of the (1×1) real-space unit cell. The entire slab (which contains the Si substrate plus a manganese silicide film on both sides of the slab) was allowed to relax until the calculated forces on each atom were smaller than 0.03 eV/Å. Three types of slab systems are studied.

(i) Clean silicon slabs with ten layers for the (111), or eight layers for the (001) surface, in order to obtain the surface energy of these silicon surfaces.

(ii) Slabs of manganese monosilicide MnSi, both in its ground state (the $B20$ phase) and in the cesium-chloride structure ($B2$ phase). Surface energies were calculated for the (111) and $(\bar{1}\bar{1}\bar{1})$ surfaces of the $B20$ phase, and for both the (001) and (111) surfaces of the $B2$ phase. Inversion symmetry for the $B2$ structure ensures that the surface energies for its (111) and $(\bar{1}\bar{1}\bar{1})$ surfaces are equal. For the $B20$ structure, we use a slab with (111) surface normal and inequivalent top

and bottom surfaces of the slab. Thus, the average of the (111) and $(\bar{1}\bar{1}\bar{1})$ surface energies is obtained,²⁵ which turns out to be sufficient for the considerations in this work.

(iii) Slab models of the Si(111) surface covered by thin films of MnSi of various thickness, either in the $B20$ structure or the $B2$ structure. Specifically, we use three-dimensional periodic supercells made of ten Si layers and up to 12 layers of alternating Mn and Si atomic planes along the (111) direction on both sides of the slab. For details concerning the calculations of MnSi thin films on Si(001), we refer to our earlier published work.^{5,8}

Tests performed for the thickness of the supercell proved that the considered number of layers was sufficiently large to reproduce bulklike behavior in the central layers. In order to compare the structural stability of the clean surfaces and of different films, surface energies (for the bare surfaces) or formation energies (for thin films) are calculated by *ab initio* thermodynamics.²⁶ In this approach, surface energies are calculated under the assumption that the surface is in thermodynamic equilibrium with the respective bulk material. For the surfaces of elemental silicon, the surface energy (at zero temperature and pressure) is thus independent of the chemical potential, and only depends on the surface orientation

$$\gamma_{\text{substrate}} = [E^{\text{tot}} - N_{\text{Si}}\mu_{\text{Si}}]/A, \quad (1)$$

where E^{tot} is the total energy of the slab (relative to isolated atoms) $\mu_{\text{Si}} = -E_{\text{Si}}^{\text{coh}}$, the cohesive energy of Si in the diamond structure, N_{Si} is the number of silicon atoms in the supercell, and A is the area of the surface unit cell.

The surface energies of a compound material, such as MnSi, depend on an additional variable, namely, the chemical potential of manganese μ_{Mn} :

$$\gamma_{\text{surface}}^{\text{MnSi}}(\mu_{\text{Mn}}) = [E^{\text{tot}} - N_{\text{Si}}\mu_{\text{MnSi}} - (N_{\text{Mn}} - N_{\text{Si}})\mu_{\text{Mn}}]/A, \quad (2)$$

where $\mu_{\text{MnSi}} = -E_{\text{MnSi}}^{\text{coh}}$ and N_{Mn} is the number of manganese atoms in the slab. In practice, the value of μ_{Mn} will depend on the chemical environment in which the surface is prepared. However, there are limits for the value of μ_{Mn} under thermodynamic equilibrium conditions. In one limiting case, the surface is in equilibrium with a reservoir of bulk manganese

$$\mu_{\text{Mn}} \leq -E_{\text{Mn}}^{\text{coh}}. \quad (3)$$

For the cohesive energy of bulk Mn $E_{\text{Mn}}^{\text{coh}}$, we substitute the energy of the ground state α -Mn, obtained by applying a correction of -0.07 eV per Mn atom²⁷ to the cohesive energy of γ -Mn (fcc structure) calculated by WIEN2K. In the other limit, the surface is in equilibrium with a reservoir of bulk silicon. This leads to an estimate for the minimum value of μ_{Mn} ,

$$\mu_{\text{Mn}} \geq -E_{\text{MnSi}}^{\text{coh}} + E_{\text{Si}}^{\text{coh}}. \quad (4)$$

For films on a substrate, we define the formation energy as the energy required to form the film from elemental reservoirs of its constituents on the clean (but possibly reconstructed) surface of the substrate

$$E^{\text{form}} = \frac{1}{2A} \left(E^{\text{tot}} - \sum_i N_i \mu_i \right) - \gamma_{\text{substrate}}^{(j)}. \quad (5)$$

Here E^{tot} , N_i and μ_i refer to total energy of the slab per (1×1) supercell, the number of atoms of species i in the (1×1) supercell ($i = \text{Mn, Si}$), and chemical potential of these atomic species. In the last term, $\gamma_{\text{substrate}}^{(j)}$ represents the surface energy of either the Si(001) or the Si(111) surface, depending on the substrate orientation used to deposit the thin film, and A is the area of the respective (1×1) nonreconstructed unit cell. For formation of the film from elemental reservoirs (Mn and Si), the chemical potentials are set equal to the cohesive energies of the respective bulk materials $\mu_{\text{Si}} = -E_{\text{Si}}^{\text{coh}}$, $\mu_{\text{Mn}} = -E_{\text{Mn}}^{\text{coh}}$. In the following, this way of preparing the films, under excess of elemental Mn, is referred to as “Mn-rich regime.” Alternatively, we discuss a situation where the thin film is formed from reservoirs of bulk Si and bulk MnSi. In this case, referred to as the “Mn-poor regime,” the values to be inserted in Eq. (5) are $\mu_{\text{Si}} = -E_{\text{Si}}^{\text{coh}}$, $\mu_{\text{Mn}} = -E_{\text{MnSi}}^{\text{coh}} + E_{\text{Si}}^{\text{coh}}$. We note that the formation energy of the thin film contains energetic contributions from both the surface of the film, its interface with the substrate, and the strain energy due to lattice mismatch between the film material and the substrate. Both for the $B2$ phase and for the $B20$ phase of MnSi, the calculated lattice mismatch with silicon is 2.2 and 4.9% [experimental value: 3.2% (Ref. 28)], respectively. For the films considered here, with a coverage of up to three monolayers (ML), the energy due to the elastic distortion of the epitaxial films are small. We estimate this elastic energy by performing DFT calculations of appropriately distorted bulk unit cells of MnSi, and find the elastic energies to be less than $2 \text{ meV}/\text{\AA}^3$ for the largest mismatch, 4.9% for $B20/\text{Si}(111)$, and smaller for the other film-substrate combinations.

Finally, we define the interface energy $\gamma_{\text{interface}}$ between the thin films and the substrate, using the formation energy and the surface energy introduced above. Since the epitaxial strain contributions are small, we can neglect them here, and express the interface energy approximately as

$$\gamma_{\text{interface}} = E_{\text{form}} - \gamma_{\text{surface}}^{\text{MnSi}}. \quad (6)$$

Since all quantities in this expression depend on the chemical potential of manganese, it is important that both E_{form} and $\gamma_{\text{surface}}^{\text{MnSi}}$ are evaluated for the same value of μ_{Mn} . In the following, surface and interface energies of films with $B2$ -like structure are quoted for $\mu_{\text{Mn}} = -E_{\text{MnSi}, B2}^{\text{coh}} + E_{\text{Si}}^{\text{coh}}$, i.e., with respect to a reservoir of (hypothetical) bulk MnSi in the $B2$ crystal structure. For films with a $B20$ -like structure γ_{surface} and $\gamma_{\text{interface}}$ are quoted with μ_{Mn} determined by a reservoir of the $B20$ phase of bulk MnSi.

III. Mn-SILICIDE FILMS ON Si(111)

A. Films with $B20$ -like structure

Manganese monosilicide is known to crystallize in a cubic crystal structure with four Mn and four Si atoms per unit cell,²⁹ the $B20$ structure. The point group of this crystal structure is $P2_13$, i.e., it possesses four threefold rotational

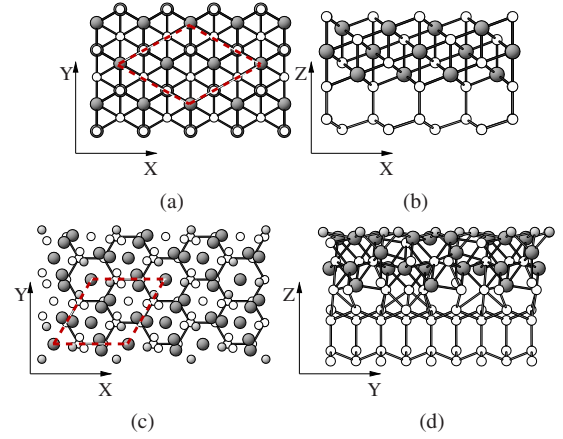


FIG. 1. (Color online) MnSi film with $B2$ structure (a) in top view and (b) in side view, and with $B20$ structure (c) in top view and (d) in side view. In the top views, the $\sqrt{3} \times \sqrt{3}$ cell is indicated by dashed (red) lines. Small balls represent Si atoms (with top-layer atoms shaded), and large dark balls Mn atoms. The hexagonal bonding pattern in (c) displays the Si substrate lattice.

axes, pointing in the cubic (111) , $(\bar{1}\bar{1}\bar{1})$, $(\bar{1}\bar{1}\bar{1})$, and $(\bar{1}\bar{1}\bar{1})$ directions. A (111) film of MnSi can be matched epitaxially with the Si(111) surface. The (1×1) surface unit cell of MnSi(111) is similar in size to the $(\sqrt{3} \times \sqrt{3})$ unit cell of Si(111): The mismatch amounts to 3.2% for the experimental, or 4.9% for our calculated lattice constants of the two bulk materials. A (111) slab of MnSi in the $B20$ structure consists of alternating layers of Mn and Si atoms with a repetition period of 12 layers. Groups of four layers follow each other in an $ABCABC\dots$ stacking sequence. Each such four-layer group consists of a “dense” Mn layer, a “sparse” Si layer, a “sparse” Mn layer, and a “dense” Si layer. Dense and sparse layers have three and one atom per (1×1) unit cell of MnSi(111), respectively.

We performed total-energy DFT calculations for several thin film structures of MnSi on Si(111). The lateral size of the unit cell used for the Si substrate was $\sqrt{3} \times \sqrt{3}$ in terms of the ideal Si(111) surface unit mesh. Since the $B20$ structure of MnSi is more close packed than the diamond structure of silicon, we define one monolayer of manganese by having two Mn atoms per surface Si atom. The film structures investigated contained one dense layer of Mn with three Mn atoms (corresponding to 0.5 ML), or two dense plus two sparse layers of Mn with a total of eight Mn atoms (4/3 ML). In the latter case, the interface is formed by a dense layer of Si, where each Si atom makes one vertical bond to a Si substrate atom. In both cases, the surface is terminated by a dense layer of threefold-coordinated Si atoms. This termination is supported by the analysis of x-ray photoemission experiments²⁰ indicating the presence of surface Si atoms. The atomic structure of this film is shown in Fig. 1(c) in top view and in Fig. 1(d) in side view.

Thermodynamic stability. In Table I, the formation energy of the $B20$ film corresponding to a Mn coverage of $\theta = 4/3$ ML, as well as the interfacial, surface and central layer(s) spin magnetic moments inside of muffin-tin sphere²⁵ are listed. The calculations show that the $B20$ -like film, having a

TABLE I. Formation energy E_{form} with respect to reservoirs of elemental Mn and Si, and average spin magnetic moment per Mn atom in the interface (M_I), surface (M_S) and central layers (M_C) of MnSi epitaxial films on Si(111) with B_2 structure (1.5 ML Mn coverage) and $B20$ structure (4/3 ML Mn coverage).

structure	ΔE meV/Å ²	M_I μ_B/Mn	M_S μ_B/Mn	M_C μ_B/Mn
$B2$	-44	1.5	1.9	0.7
$B20$ (FM)	-76	3.4	2.3	0.9 0.02
$B20$ (AFM)	-76	-3.4	2.4	-0.1 0.04

formation energy of -76 meV/Å², is most stable among the structures studied. The minus sign indicates that formation of such a film from elemental Mn and Si is exothermic. This is in line with the experimental observation of $\sqrt{3} \times \sqrt{3}$ -reconstructed islands²¹ or films^{12,20} indicative of MnSi in the $B20$ structure. In these experiments, flat extended islands several tens of nm in diameter and about 4, 8, or 12 Å in height (Ref. 12), or flat, about 10 nm wide islands near step bunches (Ref. 21) had been observed in STM images after depositing Mn on Si(111) and annealing to 350–450 °C. Furthermore, our calculations clearly show that formation of a pure Mn film would be energetically very unfavorable, with a formation energy of 292 meV/Å², similar to our previous findings for Mn/Si(001).⁵

Despite the lattice mismatch between the $B20$ structure and silicon, transmission electron microscopy images show that thin films of MnSi (<16 ML of Mn) can be grown epitaxially.¹⁶ For similar films grown with Bi as a surfactant, a hexagonal superstructure with a period of about 100 Å superimposed on the $\sqrt{3} \times \sqrt{3}$ reconstruction was detected by SPA-LEED and STM.¹⁷ For thicker films, it is observed experimentally that the lattice mismatch between the $B20$ structure and silicon induces a long-range dislocation network.²⁰ Since we are interested in very thin films, our calculations assume a perfect epitaxial relationship, and ignore imperfections of the interface related to these long-range structures. With these limitations in mind, we believe that the atomic structure of the $\sqrt{3} \times \sqrt{3}$ -reconstructed islands observed in Refs. 12, 20, and 21 is similar to our calculated structure, Fig. 1(c). The top-most layer in our structural model consists of threefold coordinated Si atoms with one dangling bond each. As we have shown recently by comparing simulated and measured STM images for Mn/Si(001),³⁰ filled-state STM images in this system map the dangling bonds of surface Si atoms, while subsurface Mn atoms remain invisible and are detectable only indirectly by their effect on the electronic structure. In the experimental STM images, a single structural feature with $\sqrt{3} \times \sqrt{3}$ periodicity was observed.¹² This could be tentatively ascribed to the triangle of the three surface Si atoms centered at the corner of the unit cell in Fig. 1(c). However, we cannot be conclusive about the structure of the (dense or sparse) Mn subsurface layers, since there is no experimental data that would allow to compare the position of subsurface atoms between our calculations and experiment.

Magnetic properties. For the magnetic structure of the

$B20$ -type film corresponding to 4/3 ML Mn coverage, we find a structure with all spin magnetic moments of the Mn atoms aligned in parallel and a structure with partial compensation of the spin moments to be almost energetically degenerate within the accuracy of our calculations. In the calculation with all spin magnetic moments of the Mn atoms aligned in parallel, these moments (inside the muffin-tin sphere of the Mn atoms) are found to be 2.3, 0.9, 0.02, and $3.4\mu_B$ per Mn atom at the surface, the two central, and the interface layers, respectively. For the dense layers of the $B20$ -type film, the quoted numbers are averages of the three Mn atoms per dense layer. The Si atoms in MnSi are found to have small induced magnetic moments aligned antiparallel to the Mn magnetic moments, with magnitudes between $-0.1\mu_B$ and $-0.02\mu_B$. This observation points to the fact that the magnetic coupling in MnSi films originates from $sp-d$ exchange mediated by bands with silicon sp -orbital character, as described previously.^{5,31} The total magnetic moment of the film at 4/3 ML coverage amounts to $12.5\mu_B$ per $\sqrt{3} \times \sqrt{3}$ unit cell. The state with antiparallel alignment of the Mn spin magnetic moments, being only slightly higher in energy, has similar magnitude of the magnetic moments at the surface and interface Mn atoms, but very small magnetic moments ($\leq 0.1\mu_B$) in the central layers. For both types of magnetic ordering, the magnetic moments at the surface and interface are considerably higher than the spin magnetic moments of Mn atoms in bulk MnSi, which were reported to be $\sim 0.4\mu_B$ from experiments.³² The spin polarization at the Fermi level, calculated from the density of states, is about 50%.

B. Films with $B2$ -like structure

It is well known that epitaxial thin films sometimes grow pseudomorphically, i.e., with a crystal structure different from the bulk. Due to epitaxial strain and/or contributions from the interface and surface free energy, thin films with an unusual crystal structure may become lower in energy and thus be more stable than films with the known bulklike structure. As we proposed previously,^{5,8} MnSi could possibly be grown pseudomorphically on Si(001) in the cesium-chloride structure ($B2$ structure). Experimentally, such a structure has been stabilized for Fe and Co monosilicide by epitaxial growth on Si(111), using molecular beam epitaxy (MBE).³³ In addition to the $B20$ structure, we therefore investigate the structural stability of the $B2$ structure for epitaxial films of MnSi on Si(111). We note that the $B2$ structure can be matched epitaxially with both the Si(111) and the Si(001) surface. As reported before for epitaxial MnSi films on Si(001),^{5,6,8} matching is achieved by rotating the cubic unit cell of the $B2$ structure by 45° with respect to the Si(001) (1×1) surface unit cell. The (111) plane of the $B2$ structure can be matched directly with the Si(111) surface using the (1×1) surface unit cells of both materials. In the $B2(111)/\text{Si}(111)$ films, the Mn and Si layers of the film have the same atomic density as the substrate. Figure 1(a) and 1(b) show an example for 1.5 ML coverage. Following our previous results obtained from DFT calculations for MnSi/Si(001),⁵ where a capping layer of (fourfold coordi-

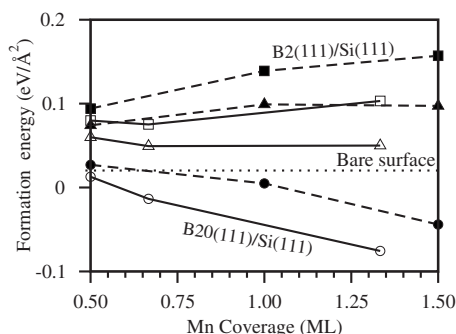


FIG. 2. Formation energy of ultrathin films with $B2$ (dashed lines, filled symbols) and $B20$ (solid lines, hollow symbols) structure of Mn monosilicide on Si(111) as a function of the deposited amount of Mn. The energy of film formation is calculated by assuming equilibrium either with the $B20$ bulk structure of Mn monosilicide (squares), or the $B2$ structure of Mn monosilicide (triangles), or Mn bulk (circles). The surface energy of the bare, unreconstructed Si(111)(1×1) surface (dotted line) is chosen as energy zero.

nated) Si adatoms was found to increase the stability of the films, all structures are considered to be covered with a capping layer of Si (threefold coordinated).

Thermodynamic stability. We compare the formation energy of the ultrathin films with $B2$ and $B20$ structure as a function of coverage up to 1.5 ML in Fig. 2. The films with $B2$ structure have generally a higher formation energy than those with the $B20$ structure, i.e., they are only metastable. With respect to bulk MnSi, the formation energies of all film are higher than the energy of the bare Si(111) surface. This implies that there is no wetting of the Si(111) surface by MnSi; instead, growth via formation of MnSi islands is to be expected.

Magnetic properties. The values of the surface and interface spin magnetic moments are found to be somewhat lower in the film with $B2$ -like structure compared to the $B20$ -like structure at similar coverage (see Table I). For the $B2$ -like film, a considerable magnetic moment ($0.7\mu_B$) is also found for the Mn atom in the central layer. Comparing to the ideal cubic $B2$ bulk structure, which is found to be nonmagnetic in our calculations,^{34,35} such an increased magnetic moment may (at least partially) be attributed to the effect of the tetragonal lattice distortion in the film on the electronic band structure close to the Fermi energy: The vertical distance between layers is about 0.84 \AA which is 5% larger than for the $B2$ bulk phase. Moreover, the magnetic moments of individual atoms are related to their coordination and bond length: The Mn atoms in the surface and interface layer make seven bonds with Si atoms at distances between 2.38 and 2.5 \AA , while the Mn atoms in the central layer have eight bonds to Si atoms. The bonds between the Si substrate and Mn interface layer are slightly shorter than the Mn-Si bonds in the central layers. Consequently, there is stronger orbital mixing between electronic states at the interface, consistent with the smaller spin magnetic moment of the Mn at the interface (M_I in Table I) compared to the surface (M_S in Table I). For the $B2$ -like film at 1.5 ML coverage, the total magnetic moment amounts to $4.5\mu_B$ per 1×1 unit cell. The

spin polarization at the Fermi level, calculated from the density of states, is 59% for this Mn coverage.

In order to check if these magnetic properties persist for thicker films, we calculated MnSi films with $B2$ -like structure corresponding to $\theta=3$ ML coverage. It is found that the magnetic moments of the Mn atoms at the surface and interface are still large ($1.8\mu_B$ and $-2.0\mu_B$, respectively), but now antiparallel alignment between the surface and interface magnetic moments is energetically preferred. This finding is analogous to our previous results for 3 ML of MnSi on Si(001).⁵ In the 3 ML-thick $B2$ -like film on Si(111), the magnetic moment of the Mn atoms gradually changes from layer to layer when going from the interface to the surface. In the two central layers, where the magnetic moment changes sign, its absolute value is only about $0.2\mu_B$. However, from analyzing the partial density of states, we find that the 3 ML film still has a rather high spin polarization at the Fermi level for both the interface and surface layer of 70 and 84%, respectively. In our previous study of a 3 ML MnSi film on Si(001), this quantity had been found to be 27% only.⁸

In summary, we find that a homogenous MnSi film on the Si substrate is thermodynamically metastable, since it is the most stable film structure, but still higher in energy than large three-dimensional (3D) islands with MnSi bulk structure. From the structures studied here, we conclude that islands with a $(\sqrt{3} \times \sqrt{3})R30^\circ$ surface reconstruction are most favorable. For such islands, considerable magnetic moments at the interface and surface Mn atoms and a high degree of spin polarization at the Fermi level are predicted. Both for the films with the $B2$ and $B20$ structure with coverage ≤ 1.5 ML, ferromagnetic ordering is found to be (slightly) more favorable than other magnetic structures that we have tested in our calculations. Experimentally, there is no clear evidence yet for ferromagnetism in MnSi films. However, magneto-optic Kerr effect measurements¹⁶ have found deviations from a Curie-Weiss law of the magnetic susceptibility. For the applicability of this material in spintronics devices, a key quantity is the interface spin polarization at the Fermi level. For the films predicted to be ferromagnetic, the values are comparable to the spin polarization of, e.g., bulk iron of about 60%.³⁶

IV. FORMATION OF 3D ISLANDS

As discussed above, thin MnSi films tend to transform to 3D structures. However, formation of side facets at 3D islands costs additional surface energy. Therefore, 3D islands will be energetically favorable only if the islands exceed a certain size, corresponding to a certain coverage of manganese (at a given island density). In the following, we give an estimate for the minimum size of a stable island of MnSi on both the Si(001) and the Si(111) substrates. This analysis follows thermodynamic arguments in the spirit of the thermodynamic nucleation theory of Gibbs and Volmer and Becker and Döring.^{37,38} It is expected to apply to situations close to thermodynamic equilibrium, where the critical nucleus consists of a large number of atoms. For example, the critical nucleus for Si homoepitaxy on Si(001) was found to consist of ~ 650 dimers at the typical growth temperature

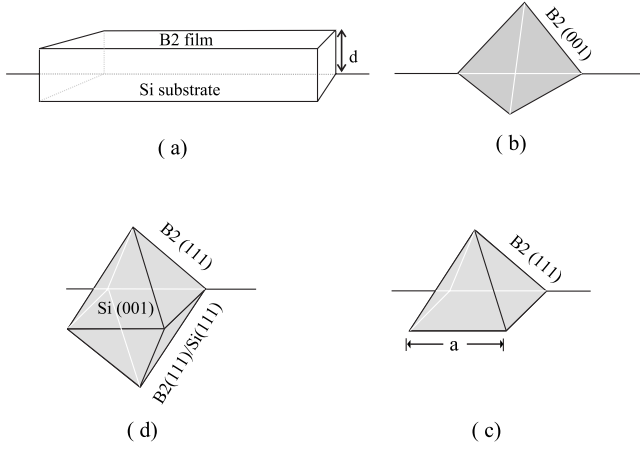


FIG. 3. Schematic illustration of (a) formation of a film with thickness d and (b) island formation with island base length a . On the Si(111) substrate, tetrahedral islands with $B2(001)$ facets (b) will form, whereas pyramid islands (c) with $B2(111)$ facets will form on the Si(001) substrate. The “iceberg” island (d) with $B2$ structure can form on both Si substrates.

of 650 °C (Ref. 39). This regime is in contrast to nucleation far from equilibrium: experiments performed under such conditions suggest that nucleation proceeds via small clusters²¹ whose size and shape are closely related to the Si(111) (7×7) reconstruction.

For simplicity, we restrict our analysis to structures with (001) or (111) surfaces or interfaces. Realistic island shapes are more complex (see, e.g., Refs. 21 and 22), and have additional facets. However, already the assumed simple island shape allows for a preliminary estimate of the differences in the stable island size on Si(001) and Si(111). Specifically, we consider pyramid-shaped islands of MnSi with a square base [for Si(001) substrate], or triangular base [for Si(111) substrate], both with base length a . Figure 3 schematically illustrates island formation on both substrates. It is supposed that the island forming on Si(001) has two $\{111\}$ and two $\{\bar{1}\bar{1}\bar{1}\}$ facets, and the tetrahedral island on Si(111) has three $\{001\}$ facets, cf. Fig. 3. For Si(001), we additionally consider bipyramids (with an inverted pyramid extending into the substrate), in the following called “iceberg,” see Fig. 3(d), with both $\{111\}$ and $\{\bar{1}\bar{1}\bar{1}\}$ interfaces between the island and the substrate. In general, the material in the island is assumed to have the $B2$ crystal structure, whose (001) and (111) surface and interface energies we have calculated in this work. For the iceberg island on Si(001) with only $\{111\}$ and $\{\bar{1}\bar{1}\bar{1}\}$ surfaces and interfaces, we are in position to consider the $B20$ structure for the island material, too.

Next, we calculate the energy difference ΔE between the MnSi island (on an otherwise clean, reconstructed substrate surface) and a hypothetical homogeneous film of MnSi containing the same amount of Mn. The thickness of such a film is denoted by d , see Fig. 3(a). We are primarily interested in the stability of films with the $B2$ structure with respect to island formation. Therefore this structure is assumed for the film. ΔE can be written as

TABLE II. Film thickness d (Å) for an MnSi film formed after deposition of 3 ML of manganese, facet area A_{facet} , energy of film formation per area γ_{film} (meV/Å²), and surface energy of the bare surface $\gamma_{\text{substrate}}$ (meV/Å²). For Si, reconstructed surfaces are considered, while for MnSi relaxed (1×1) surfaces are considered, ignoring possible (hitherto unknown) reconstructions.

Film	d Å	A_{facet}	γ_{film} meV/Å ²	$\gamma_{\text{substrate}}$ meV/Å ²
$B2(001)/\text{Si}(001)$	7.51	$(\sqrt{3}/4)a^2$	219	84
$B2(111)/\text{Si}(111)$	8.87	$(1/4)a^2$	200	81
$B20(111)/\text{Si}(111)$	8.00	$(1/4)a^2$	203	81

$$\Delta E = E_{\text{film}} - E_{\text{island}} - \epsilon V, \quad (7)$$

where E_{film} is the formation energy of a film covering an area A_{film} , E_{island} is the energy associated with formation of an island of volume V , and the last term ϵV accounts for energy changes associated with a possibly different crystal structure of the film and the island. This term is important if the $B2$ -like film transforms into an island of $B20$ structure. In this case, $\epsilon = 11 \text{ meV}/\text{Å}^3$ is the difference in the specific formation enthalpy of the two structures per molar volume of MnSi. Moreover, also the strain state of the film and the island will generally differ. However, due to the good lattice match of both the $B2$ and the $B20$ structure with Si, the contribution from strain is small $\epsilon < 2 \text{ meV}/\text{Å}^3$ and therefore neglected in the following. The first two contributions to ΔE in Eq. (7) are given by

$$E_{\text{film}} = A_{\text{film}} \gamma_{\text{film}}, \quad (8)$$

$$E_{\text{island}} = (A_{\text{film}} - A_{\text{interface}}) \gamma_{\text{substrate}} + A_{\text{interface}} \gamma_{\text{interface}} + N A_{\text{facet}} \gamma_{\text{surface}}^{\text{MnSi}}. \quad (9)$$

Here γ_{film} is the formation energy of the film per unit area, as defined in Eq. (5). N is the number of facets of the island and A_{facet} is their area. These two quantities follow from geometrical considerations, and are given in Table II. Likewise, the area $A_{\text{interface}}$ of the interface between substrate and island is determined geometrically, and specified in Table III. $\gamma_{\text{substrate}}$ and $\gamma_{\text{surface}}^{\text{MnSi}}$ are the surface energy of the bare substrate and of the island facets. Both quantities are obtained from our DFT calculations according to Eq. (1) and (2). Their values are summarized in Table IV. Note that γ_{form} and $\gamma_{\text{interface}}$ are evaluated with respect to being in equilibrium with the MnSi structure of the corresponding island, i.e., $\mu_{\text{Mn}} = -E_{\text{MnSi},j}^{\text{coh}} + E_{\text{Si}}^{\text{coh}}$, where $j = (B2, B20)$, depending on the crystal structure of MnSi in question. In general, Eq. (9) gives a lower bound for the energy of island formation, since the additional energy cost associated with the formation of edges and/or with imperfect surface reconstructions on very small facets has been omitted. However, for larger islands, these contributions are negligible compared to the surface contribution (see, e.g., the discussion in Ref. 40 for InAs islands).

Due to mass conservation, the island base a , film thickness d , and film area A_{film} , are related by the equation

TABLE III. Interface area $A_{\text{interface}}$, volume of the islands V_{island} , interface energy per area $\gamma_{\text{interface}}$, and stable island size a_0 . Bulk MnSi in the $B2$ structure is considered as reservoir for calculating the chemical potential of Mn.

film		$A_{\text{interface}}$ \AA^2	V_{island} \AA^3	$\gamma_{\text{interface}}$ $\text{meV}/\text{\AA}^2$	a_0 \AA
$B2(001)$	pyramid $B2$	a^2	$\sqrt{2}/6 a^3$	101	52
on	iceberg $B2$	$\sqrt{3}a^2$	$\frac{\sqrt{2}}{3}a^3$	99	27
Si(001)	iceberg $B20$	$\sqrt{3}a^2$	$\frac{\sqrt{2}}{3}a^3$	98	15
$B2(111)$	pyramid $B2$	$\frac{\sqrt{3}}{4}a^2$	$\frac{1}{12\sqrt{2}}a^3$	99	133
on	iceberg $B2$	$\frac{3}{4}a^2$	$\frac{1}{6\sqrt{2}}a^3$	101	71
Si(111)					

$$\frac{1}{6} \frac{a^3 \tan \alpha}{v_{\text{mol}}^{\text{island}}} = \frac{dA_{\text{film}}}{v_{\text{mol}}^{\text{film}}}. \quad (10)$$

Here, α is the angle between the island facets and the substrate and $v_{\text{mol}}^{\text{island}}$ and $v_{\text{mol}}^{\text{film}}$ are the molecular volumes of MnSi in the crystal structure of the island and film, respectively. The calculated volume per MnSi formula unit in the $B20$ and $B2$ crystal structures is 56.08 and 43.68 \AA^3 , respectively.

Solving the above equation for A_{film} and inserting the resulting expression into Eq. (8) allows us to eliminate this quantity. The total energy difference between film and island per unit volume can be expressed as

TABLE IV. Surface energy γ_{surface} ($\text{meV}/\text{\AA}^2$) of the nonreconstructed Si(001) and Si(111) surfaces and of the stable reconstructed surfaces Si(001)(2×2) and Si(111)(7×7). The GGA-PBE value for the surface energy of the reconstructed Si(111)(7×7) is extrapolated from LDA calculations using ultrasoft pseudopotentials (Ref. 41) by comparing the surface energies of smaller cells in both methods. Moreover, surface energies of MnSi in the $B2$ structure are given for the unreconstructed (001) and (111) (1×1) surfaces. For MnSi in the $B20$ structure, the quoted number is the average surface energy of the (111) and the ($\bar{1}\bar{1}\bar{1}$) surface. Bulk MnSi in the $B2$ structure is considered as a reservoir for the chemical potential of Mn.

surface	surface energy ($\text{meV}/\text{\AA}^2$)
Si(001)(1×1)	136
Si(001)(2×2)	84
Si(111)(1×1)	100
Si(111)(7×7)	81
MnSi($B2$)(001)	118
MnSi($B2$)(111)	101
MnSi($B20$)(111)/($\bar{1}\bar{1}\bar{1}$)	105

$$\Delta E/V = (\gamma_{\text{substrate}} - \gamma_{\text{film}})(v_{\text{atom}}^{\text{film}}/v_{\text{atom}}^{\text{island}})/d + [A_{\text{interface}}(\gamma_{\text{interface}} - \gamma_{\text{substrate}}) + NA_{\text{facet}}\gamma_{\text{surface}}^{\text{MnSi}}]/V - \epsilon. \quad (11)$$

A positive value of ΔE indicates that MnSi film formation is energetically favorable compared to island formation for the specified substrate orientation and Mn coverage, while a negative value indicates the stability of the islands. The condition $\Delta E=0$, i.e., setting the right-hand side of Eq. (11) to zero, defines the volume V_0 for which the island first becomes stable. As an example, we calculate this island volume and the corresponding base length a_0 explicitly for deposition of 3 ML of manganese.

For clarity, the steps of this calculation are described in the following. First, we need to calculate the surface energy of both the Si substrates and the MnSi surfaces that appear as island side facets. The numerical results are collected in Table IV. According to our GGA-PBE calculations, the surface energy $\gamma_{\text{substrate}}$ of the Si(111) surface is less than that of Si(001), both in the reconstructed and in the unreconstructed case. This is in agreement with the results of previous LDA calculations.⁴¹ Similarly, the (111) surface of MnSi films with $B2$ structure is found to be somewhat more stable than the (001) surface. The average surface energy of the (111) and ($\bar{1}\bar{1}\bar{1}$) surfaces of MnSi in the $B20$ phase is comparable to the same surfaces of the $B2$ phase. The lower surface energies of the (111)-oriented surfaces compared to the (001) surface may be related to the surface termination with threefold or fourfold coordinated Si adatoms, respectively. Whereas threefold coordinated Si adatoms are low-energy motifs [see the Si(111) (7×7) reconstruction], Si atoms with four bonds all pointing into the same half-space are energetically more costly. Generally, the surface energies for MnSi, for the specified value of μ_{Mn} , are higher than those of the (reconstructed) Si surfaces of the same orientation. Under these conditions, MnSi will not form a wetting layer on silicon; we rather expect island growth in the Volmer-Weber mode for sufficiently large coverage of manganese.

Next, the values collected in Tables II and III are to be inserted into Eq. (11). Table III contains the formulas for calculating the interface area and the island volume of various cases. Moreover, the interface energy, and the final result, the base length a_0 of the smallest stable island, are given. For Si(001), we consider three possible kinds of islands, a pyramid with four (001) facets with $B2$ structure, an iceberg island with $B2$ structure and an iceberg island with $B20$ structure. For the pyramid, the interface is between the $B2(001)$ and the bare Si(001) surface. For the iceberg island, there are two (111) and two ($\bar{1}\bar{1}\bar{1}$) interfacial facets between the $B2$ (or $B20$) structure of MnSi and Si(111). Because the $B20$ structure is incompatible with (001) lattice planes of Si, the energy of such an interface is not calculated, and the formation of an iceberg island with $B20$ structure on Si(111) is discarded. The interface of a pyramid island on Si(001) is a square with a^2 , while icebergs have four interfacial facets with an area of $(\sqrt{3}/4) a^2$ each. The interface of a pyramid island on Si(111) has a triangular base with an area of $(\sqrt{3}/4)$

a^2 , while in case of the iceberg the interface area consists of three such equilateral triangles.

From the minimum stable island size a_0 (right column of Table III) the following conclusions can be drawn: On Si(001), the stable island size is generally smaller than on Si(111). Therefore Volmer-Weber growth is to be expected for MnSi on Si(001), as observed experimentally.^{22,42} In contrast, a (metastable) film of MnSi on Si(111) will only decay into islands if fluctuations during growth overcome some threshold value. As one can see from the values of the stable island size a_0 , iceberg islands with $B20$ structure on Si(001) are the smallest islands to become stable. In general, the iceberg variants of the islands are found to be more favorable than a pyramid shape on both substrates. On Si(001), the icebergs having $B20$ structure are stabilized additionally due to the transition from the $B2$ film to the $B20$ island structure. This is consistent with the observation of a $(\sqrt{3} \times \sqrt{3})$ structure on the side facets of MnSi islands on Si(001),²² indicating that the $B20$ structure has indeed formed in these islands. The base length of a stable island of the $B20$ structure on Si(001) with iceberg shape is 15 Å, which amounts to only about four surface lattice constants of Si(001), or of MnSi (in the $B20$ structure). In contrast, stable pyramid islands on Si(111) are much larger than the (7×7) unit mesh of the surface reconstruction. Their base length is about 30 times the lattice constant of MnSi in the $B20$ structure.

In a situation where Gibbs' theory of nucleation is applicable, we expect that islands nucleate more easily on the Si(001) compared to the Si(111) substrate. For an island size larger than the stable value a_0 , ΔE becomes negative, indicating that further growth of the islands is exothermic. This is in agreement with the recently observed Ostwald ripening of MnSi islands on Si(001).^{42,43}

V. SUMMARY

In summary, we have investigated the morphology of manganese monosilicide films on the Si(111) substrate by means of DFT calculations. The Si(111) substrate is compatible with Mn monosilicide in both the $B20$ and $B2$ structures, while the formerly studied Si(001) substrate only matches with the (so far not yet synthesized) $B2$ structure of MnSi. We find that the thermodynamic stability of MnSi films on Si(111) is generally higher than on Si(001). On Si(111), films with the $B20$ structure are energetically more favorable than those with $B2$ structure. A Si-capping layer is found to enhance the stability of all MnSi films investigated. Moreover, we calculate the stable island size of pyramidal or bipyramidal MnSi islands on both Si(001) and Si(111). While already very small islands with a base length of a few lattice constants (if edge energy contributions are neglected) are found to be more stable than a homogeneous film on Si(001), much large nuclei are required on Si(111) to destabilize a MnSi film. Both the MnSi films on Si(001) and Si(111) show large magnetic moments at the Mn atoms near the surfaces and interfaces. The values for the spin polarization at the Fermi level in MnSi/Si(111) are even higher than those found in our previous calculations for Mn/Si(001). Therefore we conclude that experimental preparation of an MnSi film on Si(111) is probably easier to achieve than on Si(001), and that such films could even be more useful from the viewpoint of spintronics applications.

ACKNOWLEDGMENTS

This work was in part supported by the Deutsche Forschungsgemeinschaft through SFB 290.

-
- ¹V. P. LaBella, D. W. Bullock, Z. Ding, C. Emery, A. Venkatesan, W. F. Oliver, G. J. Salamo, P. M. Thibado, and M. Mortazavi, *Science* **292**, 1518 (2001).
- ²H. J. Zhu, M. Ramsteiner, H. Kostial, M. Wassermeier, H.-P. Schönherr, and K. H. Ploog, *Phys. Rev. Lett.* **87**, 016601 (2001).
- ³M. Zwierzycki, K. Xia, P. J. Kelly, G. E. W. Bauer, and I. Turek, *Phys. Rev. B* **67**, 092401 (2003).
- ⁴B. Jenichen, V. M. Kaganer, J. Herfort, D. K. Satapathy, H. P. Schönherr, W. Braun, and K. H. Ploog, *Phys. Rev. B* **72**, 075329 (2005).
- ⁵H. Wu, M. Hortamani, P. Kratzer, and M. Scheffler, *Phys. Rev. Lett.* **92**, 237202 (2004).
- ⁶H. Wu, P. Kratzer, and M. Scheffler, *Phys. Rev. B* **72**, 144425 (2005).
- ⁷E. Şaşıoğlu, I. Galanakis, L. M. Sandratskii, and P. Bruno, *J. Phys.: Condens. Matter* **17**, 3915 (2005).
- ⁸M. Hortamani, H. Wu, P. Kratzer, and M. Scheffler, *Phys. Rev. B* **74**, 205305 (2006).
- ⁹Y. C. Lian and L. J. Chen, *Appl. Phys. Lett.* **48**, 359 (1986).
- ¹⁰Q. Zhang, M. Tanaka, M. Takeguchi, and K. Furuya, *Surf. Sci.* **508-510**, 453 (2002).
- ¹¹G. Ctistis, U. Deffke, J. Paggel, and P. Fumagalli, *J. Magn. Magn. Mater.* **240**, 420 (2002).
- ¹²M. M. R. Evans, J. C. Glueckstein, and J. Nogami, *Phys. Rev. B* **53**, 4000 (1996).
- ¹³T. Nagao, S. Ohuchi, Y. Matsuoka, and S. Hasegawa, *Surf. Sci.* **419**, 134 (1999).
- ¹⁴G. Ctistis, U. Deffke, K. Schwinge, J. J. Paggel, and P. Fumagalli, *Phys. Rev. B* **71**, 035431 (2005).
- ¹⁵U. Deffke, G. Ctistis, J. Paggel, and P. Fumagalli, *J. Appl. Phys.* **96**, 3972 (2004).
- ¹⁶K. Schwinge, C. Müller, A. Mogilatenko, J. Paggel, and P. Fumagalli, *J. Appl. Phys.* **97**, 103913 (2005).
- ¹⁷K. Schwinge, J. Paggel, and P. Fumagalli, *Surf. Sci.* **601**, 810 (2007).
- ¹⁸S. M. Shivaprasad, C. Anandan, S. G. Azatyan, Y. L. Gavriljuk, and V. G. Lifshits, *Surf. Sci.* **382**, 258 (1997).
- ¹⁹S. Kawamoto, M. Kusaka, M. Hirai, and M. Iwami, *Surf. Sci.* **242**, 331 (1991).
- ²⁰A. Kumar, M. Tallarida, M. Hansmann, U. Starke, and K. Horn, *J. Phys. D* **37**, 1083 (2004).
- ²¹S. Azatyan, M. Iwami, and V. Lifshits, *Surf. Sci.* **589**, 106 (2005).
- ²²H. Lippitz, J. J. Paggel, and P. Fumagalli, *Surf. Sci.* **575**, 307

- (2005).
- ²³J. P. Perdew, K. Burke, and M. Ernzerhof, *Phys. Rev. Lett.* **77**, 3865 (1996).
- ²⁴P. Blaha, K. Schwarz, G. K. H. Madsen, D. Kvasnicka, and J. Luitz, *WIEN2K, an Augmented Plane Wave+Local Orbitals Program for Calculating Crystal Properties*, Technische Universität Wien, Austria, 2001.
- ²⁵By comparing the total spin magnetic moment in the unit cell of the slab with the sum of the moments inside the muffin-tin spheres, we find that the interstitial space between muffin-tin spheres contributes at most 10% to the spin magnetic moment of an atom. Hence, the technical error due to the use of muffin-tin spheres only results in an underestimation of the true moments by less than 10%.
- ²⁶K. Reuter, C. Stampfl, and M. Scheffler, in *Handbook of Materials Modeling*, edited by S. Yip (Kluwer, Dordrecht, 2004), and references therein.
- ²⁷D. Hobbs and J. Hafner, *J. Phys.: Condens. Matter* **13**, L681 (2001).
- ²⁸W. B. Pearson, *Handbook of Lattice Spacing and Structures of Metals and Alloys, International Series of Monographs on Metal Physics and Physical Metallurgy* (Pergamon Press, New York, 1958). Only for the *B20* structure an experimental number is available; the *B2* structure may only exist as pseudomorphic film.
- ²⁹P. Lerch and T. Jarlborg, *J. Magn. Magn. Mater.* **131**, 321 (1994).
- ³⁰M. R. Krause, A. J. Stollenwerk, J. Reed, V. P. LaBella, M. Hortamani, P. Kratzer, and M. Scheffler, *Phys. Rev. B* **75**, 205326 (2007).
- ³¹J. Kanamori and K. Terakura, *J. Phys. Soc. Jpn.* **70**, 1433 (2001).
- ³²C. Pfleiderer, *J. Magn. Magn. Mater.* **226-230**, 23 (2001).
- ³³H. von Känel, C. Schwarz, S. Goncalves-Conto, E. Müller, L. Miglio, F. Tavazza, and G. Malegori, *Phys. Rev. Lett.* **74**, 1163 (1995).
- ³⁴M. Hortamani, L. Sandratskii, I. Mertig, P. Kratzer, and M. Scheffler (unpublished).
- ³⁵M. Hortamani, Ph.D. thesis, Freie Universität Berlin, Berlin, 2006.
- ³⁶I. I. Mazin, *Phys. Rev. Lett.* **83**, 1427 (1999).
- ³⁷R. Becker and W. Döring, *Ann. Phys.* **24**, 719 (1935).
- ³⁸R. M. Tromp and J. B. Hannon, *Surf. Rev. Lett.* **9**, 1565 (2002).
- ³⁹W. Theis and R. M. Tromp, *Phys. Rev. Lett.* **76**, 2770 (1996).
- ⁴⁰N. Moll, M. Scheffler, and E. Pehlke, *Phys. Rev. B* **58**, 4566 (1998).
- ⁴¹A. A. Stekolnikov and F. Bechstedt, *Phys. Rev. B* **72**, 125326 (2005).
- ⁴²M. R. Krause, A. J. Stollenwerk, M. Licurse, and V. P. LaBella, *J. Vac. Sci. Technol. A* **24**, 1480 (2006).
- ⁴³M. R. Krause, A. J. Stollenwerk, M. Licurse, and V. P. LaBella, *Appl. Phys. Lett.* **91**, 041903 (2007).